REPORT DOCUMENTATION PAGE

AFRL-SR-AR-TR-03-

0191

1. REPORT DATE (DD-MM-YYYY) 28-02-2003	2. REPORT TYPE Final	3. DATES COVERED (From - To) 01-12-1999 – 30-11-2002

4. TITLE AND SUBTITLE
Development of CFD Capability to Model Flexible Structures
For Simulating Carriage Loads and Store Separation
Trajectories
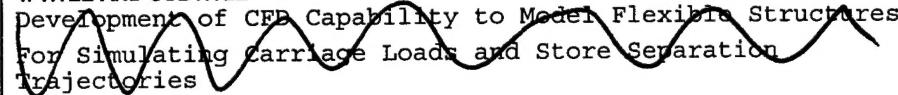
5a. CONTRACT NUMBER

5b. GRANT NUMBER
F49620-00-1-0006

5c. PROGRAM ELEMENT NUMBER

6. AUTHOR(S)
Wei Shyy

5d. PROJECT NUMBER

5e. TASK NUMBER

5f. WORK UNIT NUMBER

7. PERFORMING ORGANIZATION NAME(S) AND ADDRESS(ES)

University of Florida
Mechanical and Aerospace
Engineering
231 Aerospace Building
Gainesville FL 32611-6250

8. PERFORMING ORGANIZATION REPORT NUMBER

9. SPONSORING / MONITORING AGENCY NAME(S) AND ADDRESS(ES)
AFOSR
801 N Randolph Street
Arlington VA 22203-1977

10. SPONSOR/MONITOR'S ACRONYM(S)

11. SPONSOR/MONITOR'S REPORT NUMBER(S)

12. DISTRIBUTION / AVAILABILITY STATEMENT

Approved for Public Release; distribution is unlimited

13. SUPPLEMENTARY NOTES

14. ABSTRACT
The non-linear fluid-structure interaction problem is studied based on moving grid techniques. A closely-coupled approach is used to perform the combined fluid and structure interaction computations. The flow solver is an unsteady, implicit, three-dimensional, multi-block, pressure-based Navier-Stokes solver. The structure solver is based on either (i) a linear, time-invariant model derived via classical structural finite elements, or (ii) the flexible structural solver is based on a non-linear dynamic membrane model with the material obeying the hyperelastic Mooney's model. Suitable interfacing techniques are incorporated to couple and synchronize the flow and structure solvers. Moving boundary technique, geometric conservation laws, coupling mechanisms between fluid and structure solvers have been investigated, and appropriate techniques developed. In addition, technique such as proper orthogonal decomposition has also been investigated to address the need of information compression and data transmission. The research has been presented in various national and international conferences, and refereed journals. The detailed information is given on a separate sheet. The current research has advanced our computation and modeling capabilities for simulating carriage loads and store separation trajectories.

15. SUBJECT TERMS
computational fluid and structure dynamics, moving boundaries, dynamic simulations

16. SECURITY CLASSIFICATION OF:			17. LIMITATION OF ABSTRACT	18. NUMBER OF PAGES	19a. NAME OF RESPONSIBLE PERSON Wei Shyy
a. REPORT Unclassified	b. ABSTRACT Unclassified	c. THIS PAGE Unclassified	UL	3 + reprints	19b. TELEPHONE NUMBER (include area code) (352)392-0961

Standard Form 298 (Rev. 8-98)
Prescribed by ANSI Std. Z39.18

20030602 135

COMPUTATIONAL AEROELASTICITY USING A PRESSURE-BASED SOLVER

Ramji Kamakoti[*], Yongsheng Lian[*], Sean Regisford[*], Andrew Kurdila[†] and Wei Shyy[§]
Department of Aerospace Engineering, Mechanics and Engineering Science
University of Florida
Gainesville, FL 32611-6250

Abstract

The fluid-structure interaction problem is studied for two different wing configurations based on moving grid techniques. These configurations demonstrate the interaction between a rigid structure and fluid, as well as the interaction between a flexible structure and fluid. A loosely coupled approach is used to perform the combined fluid and structure computations. The flow solver is based on an unsteady, implicit, three-dimensional, multi-block, pressure-based Navier-Stokes solver. The rigid structural model is based on a linear, time-invariant model derived via classical structural finite elements whereas the flexible structural model is based on a non-linear dynamic membrane model with the material obeying the hyperelastic Mooney's model. A suitable interfacing technique is incorporated to couple and synchronize the flow and structure solver. We present unsteady computations performed on a $45°$ wing with sweep back as well as a membrane wing typically motivated by micro-air vehicle applications.

1. Introduction:

The interaction of aerodynamic forces and inertial forces within elastic structural systems is a well-known and difficult problem. In a coupled system, the external forces acting on a structural system such as a wing leads to a deformation in the wing geometry, and this structural deformation thereby leads to modified aerodynamic loads. While computational methods that study different aspects of aeroelastic response have been studied for some time, numerous open research issues remain to be resolved. For example, many approaches in computational aeroelasticity seek to synthesize independent computational approaches for

* Graduate student. Member AIAA

† Professor. Associate Fellow AIAA.

† Professor and Chairman. Fellow AIAA.

the aerodynamic and the structural dynamic subsystems. This strategy is known to be fraught with complications associated with the interaction between the two simulation modules. Some of the issues arise from the fact that the computational fluid dynamic (CFD) and the computational structural dynamic (CSD) mesh systems are quite different. Frequently, the former uses a Eulerian or spatially fixed coordinate system while the latter uses a Lagrangian or material fixed coordinate system. Hence, care must be taken to develop a suitable interfacing technique between the two modules. Also, since the time scales are different for the two modules, unsteady calculations are no longer straightforward.

There are at least two major classifications for computational aeroelasticity (CAE). They being coupled analysis and uncoupled analysis. The coupled analysis can be further divided into fully coupled and loosely coupled analysis. In uncoupled analysis, the fluid domain and structural system are treated as two separate modules with only external interaction between them. This method is limited to small perturbations with nominally linear structural models. In fully coupled analysis, the governing equations for fluids and structures part are combined into one set of equations and these equations are subsequently solved and integrated in time simultaneously. Since the matrices associated with structures are an order of magnitude stiffer than those associated with fluids, it is virtually impossible to solve the entire system using a single numerical scheme. However, some methods have been developed using fully coupled methods, but are mainly restricted to 2-D problems. In the loosely coupled approach, the fluid domain and structural system are modeled in separate domains but they reside in the same module. The exchange of information between these modules takes place at the interface or the boundary. The coupling is integrated thereby allowing the two modules to exchange information at the boundaries in an efficient manner.

Several models have been developed over the years to solve various problems in aeroelasticity and address

American Institute of Aeronautics and Astronautics

several issues discussed thus far. A few of them are discussed next

Cunningham et al. (1988) developed a computational scheme for transonic aeroelastic analysis using the transonic small disturbance (TSD) formulation. The equations of motion were based on the natural vibrational modes of the aircraft. Robinson et al. (1991) developed a model along the same lines but made use of deforming mesh scheme. This technique of using TSD formulation fails when there is a strong shock or when the viscous effects dominate. To overcome this, Schuster et al. (1990) came up with a model that uses a 3-D flow solver coupled with a linear static structure model to study the aeroelastic analysis of a fighter aircraft. Grid deflection method was used to update the grid after each time step. This method was limited to static analysis. Lewis and Smith (1998) extended this method using shell finite element structures to study flutter in an engine liner.

Guruswamy and Byun (1993, 1995) developed a method by directly coupling Euler/Navier-Stokes equations for fluids with plate/shell finite element structures. A domain decomposition method, wherein fluids and structures modules are solved in separate modules, is used in this regard. The transformation of loads from CFD mesh to CSD mesh is done by bilinear interpolation and virtual surface methods. Bhardwaj et al. (1998) developed a coupling procedure that combines a variety of CFD and CSD codes. This was again limited to only static analysis. Patil et al. (1999, 2000) developed a theoretical as well as computational non-linear aeroelastic model for high aspect-ratio wings. They used the mixed variational formulation of beams in moving frames. Garcia and Guruswamy (1999) developed a coupled model of Navier-Stokes flow model with beam finite element model to perform static aeroelastic analysis of high aspect-ratio wings. Farhat and Lesoinne (2000) developed a serial as well as a parallel algorithm for nonlinear transient aeroelastic problems. They used the Arbitrary Lagrangian Eulerian (ALE) formulation with a deforming mesh algorithm for grid movement. Soulaimani (2000) developed a FEM based solver for 3-D Euler and Navier-Stokes flow equation coupled with a commercial FEM code for nonlinear CAE. A brief summary of a few models explaining the salient features like the flow solver, structural solver used, etc and the test cases used to relate the models is presented in Table 1.

However, there are quite a few limitations encountered in these models. A few of them are listed here.

- Use of Euler equations for the CFD module: This eliminates the inclusion of viscous effects, which plays an important role in aerodynamics
- Inability to predict separation in the CFD code
- Absence of moving boundary capability
- Coupled models that primarily treat 2-D cases
- Inaccurate interfacing techniques
- Modeling the wing via plate/shell structures that leads to negligence of 3-D effects

Our present model makes use of the loosely coupled approach that synthesizes a multi-block 3-D CFD solver and a linear, time-invariant structural model. The CFD code addresses the full 3-D Navier-Stokes equations along with well-validated turbulence models. The solver also has the capability to include effects for multi-block moving boundary treatment. We use linear interpolation and extrapolation techniques to carry out the interfacing between the two modules. The motivation for this work is to expand our well-validated CFD approach to study coupled aeroelastic models and consider the complexity of coupling procedures in 3-D wing models.

The main objective of this work is to study the fluid-structure interaction problem for 3-D wing geometries. We consider the AGARD 445.6 wing (Yates, 1987) and a membrane wing motivated by micro-air vehicle applications (Ifju et al., 2002) to demonstrate our methodology.

Numerous papers have been published about the various calculations done for this test-bed wing (Bennet and Edward, 1998). A brief description of the existing methods and the features addressed in our model is shown in Table 1. As can be seen from the table, our model incorporates all the key features that go into a CAE model viz., well-defined flow solver with moving mesh techniques and turbulence models, a separate structural solver and an interfacing technique that combines these two. Most of the models, until recently, used the same grid for both CFD and CSD computations. Recently, Liu et al (2000) developed a model for the AGARD wing which uses separate grids with a corresponding interfacing between them and presented solutions using the Euler equations for flow module. We choose this as our benchmark model but we use the full Navier-Stokes solutions, neglecting compressibility effects, for our flow module. We present the interfacing techniques developed thus far using the linear time-invariant structure model for the AGARD wing model as well as the membrane model on a mAV wing.

2. Numerical Procedure

2.1 Flow Solver:

A pressure-based numerical procedure presented (Shyy, 1994; Shyy et al. 1997) for curvilinear coordinates is adopted as the flow solver (STREAM). It solves the full Navier-Stokes equations for 3-D incompressible flows. The equations read as follows:

$$\frac{\partial(J\rho u)}{\partial t} + \frac{\partial(\rho U u)}{\partial \xi} + \frac{\partial(\rho V u)}{\partial \eta} + \frac{\partial(\rho W u)}{\partial \gamma}$$

$$= \frac{\partial}{\partial \xi}[\frac{\mu}{J}(q_{11}u_\xi + q_{12}u_\eta + q_{13}u_\gamma)]$$

$$+ \frac{\partial}{\partial \eta}[\frac{\mu}{J}(q_{21}u_\xi + q_{22}u_\eta + q_{23}u_\gamma)]$$

$$+ \frac{\partial}{\partial \gamma}[\frac{\mu}{J}(q_{31}u_\xi + q_{32}u_\eta + q_{33}u_\gamma)]$$

$$- [\frac{\partial}{\partial \xi}(f_1 p) + \frac{\partial}{\partial \eta}(f_4 p) + \frac{\partial}{\partial \gamma}(f_7 p)]$$

$$+ G_1(\xi,\eta,\gamma).J \tag{1}$$

$$\frac{\partial(J\rho v)}{\partial t} + \frac{\partial(\rho U v)}{\partial \xi} + \frac{\partial(\rho V v)}{\partial \eta} + \frac{\partial(\rho W v)}{\partial \gamma}$$

$$= \frac{\partial}{\partial \xi}[\frac{\mu}{J}(q_{11}v_\xi + q_{12}v_\eta + q_{13}v_\gamma)]$$

$$+ \frac{\partial}{\partial \eta}[\frac{\mu}{J}(q_{21}v_\xi + q_{22}v_\eta + q_{23}v_\gamma)]$$

$$+ \frac{\partial}{\partial \gamma}[\frac{\mu}{J}(q_{31}v_\xi + q_{32}v_\eta + q_{33}v_\gamma)]$$

$$- [\frac{\partial}{\partial \xi}(f_2 p) + \frac{\partial}{\partial \eta}(f_5 p) + \frac{\partial}{\partial \gamma}(f_8 p)]$$

$$+ G_2(\xi,\eta,\gamma).J \tag{2}$$

$$\frac{\partial(J\rho w)}{\partial t} + \frac{\partial(\rho U w)}{\partial \xi} + \frac{\partial(\rho V w)}{\partial \eta} + \frac{\partial(\rho W w)}{\partial \gamma}$$

$$= \frac{\partial}{\partial \xi}[\frac{\mu}{J}(q_{11}w_\xi + q_{12}w_\eta + q_{13}w_\gamma)]$$

$$+ \frac{\partial}{\partial \eta}[\frac{\mu}{J}(q_{21}w_\xi + q_{22}w_\eta + q_{23}w_\gamma)]$$

$$+ \frac{\partial}{\partial \gamma}[\frac{\mu}{J}(q_{31}w_\xi + q_{32}w_\eta + q_{33}w_\gamma)]$$

$$- [\frac{\partial}{\partial \xi}(f_3 p) + \frac{\partial}{\partial \eta}(f_6 p) + \frac{\partial}{\partial \gamma}(f_9 p)]$$

$$+ G_3(\xi,\eta,\gamma).J \tag{3}$$

where $(\xi \eta, \gamma)$ are time dependent curvilinear coordinates, e.g., $\xi = \xi(x, y, z, t)$. The dependent variables are the Cartesian velocity components, u, v, and w. U, V, and W, are the contravariant velocity components and they read as follows:

$$U = (u-\dot{x})(y_\eta z_\gamma - y_\gamma z_\eta) + (v-\dot{y})(z_\eta x_\gamma - z_\gamma x_\eta) + (w-\dot{z})(x_\eta y_\gamma - x_\gamma y_\eta) \tag{4}$$

$$V = (u-\dot{x})(y_\gamma z_\xi - y_\xi z_\gamma) + (v-\dot{y})(z_\gamma x_\xi - z_\xi x_\gamma) + (w-\dot{z})(x_\gamma y_\xi - x_\xi y_\gamma) \tag{5}$$

$$W = (u-\dot{x})(y_\xi z_\eta - y_\eta z_\xi) + (v-\dot{y})(z_\xi x_\eta - z_\eta x_\xi) + (w-\dot{z})(x_\xi y_\eta - x_\eta y_\xi) \tag{6}$$

where $\dot{x}, \dot{y},$ and $\dot{z}$ are the grid velocities which are approximated by the first order backward time difference

$$\dot{x} = \frac{x - x^0}{\Delta t} \tag{7}$$

where Δt is the fluid time step and the superscript refers to the previous time level. The transformation matrix between Cartesian and curvilinear coordinates is:

$$J = x_\xi y_\eta z_\gamma + x_\gamma y_\xi z_\eta + x_\eta y_\gamma z_\xi - x_\xi y_\gamma z_\eta - x_\gamma y_\eta z_\xi - x_\eta y_\xi z_\gamma \tag{8}$$

More detailed discussion about these equations can be found in Shyy (1994).

The solver incorporates many of the modern techniques for handling complex flow problems including multi-block methods and controlled numerical diffusion schemes for convection and pressure terms. A combined Cartesian-contravariant velocity formulation is adopted to facilitate a conservative, finite-volume formulation. The convection terms are treated using second-order upwind scheme, while the unsteady terms are treated using implicit Euler method. The remaining terms are treated using second order central difference schemes. More details about the code can be found in Thakur and Wright (1999).

2.1.1. Turbulence modeling

We use the most widely employed two-equation model

3

viz., the κ-ε model for turbulent computations. Since the standard κ-ε model is only valid in fully turbulent regions, it requires additional modeling near wall regions or in the no-slip regions. We use wall functions technique to model the near wall region. This technique uses the law of the wall as the constitutive relation between the velocity and the surface shear stress. The detailed formulation of the model can be found in Shyy et al. (1997).

2.2. Linear Time-invariant Structural Model:

A general, linear, time-invariant structural model is used in the coupled CFD-CSD method. Thus, the equations of motion that govern the structural dynamics of the wing take the well-known form:

$$[M]\ddot{q}(t)+[C]\dot{q}(t)+[K]q(t)=Q(t) \qquad (9)$$

where [M] is the mass matrix, [C] is the damping matrix, [K] is the stiffness matrix, $\mathbf{Q}(t)$ is a vector containing the generalized forces associated with aerodynamic loads, and $\mathbf{q}$ is a vector containing the generalized displacements. The structural solver integrates these equations of motion in time for one time step given the time step size, the pressures on structural nodes at the initial time for the time step, and the initial geometry of the wing.

The pressures are provided as scalar pressures located at structural grid points that were obtained and interpolated from a CFD calculation on a finer fluid grid. The geometry of the wing is defined in terms of the spatial global coordinates of each structural node, a list of pointers that show the relationship between nodes and surface elements, a list of pointers that show the relationship between surface elements and nodes, and a list of pointers that show the relationship between surface elements and super-elements.

Now, the structural model will be described in order to demonstrate how the structural solver integrates the equations of motion for a single time step. The scalar pressures, obtained from an interpolation of the pressures from a CFD calculation, are converted to pressure forces acting at each node of the structural grid. These pressure forces are the ones used to generate the aerodynamic loads on the wing, as illustrated by the equations:

$$\int_0^T Q(t)\delta q(t)dt = \int_0^T\int_S P\cdot\delta r dSdt \qquad (10)$$

$$Q_w = \int_S P_3 N_w(y)dldy \qquad (11)$$

$$Q_\theta = \int_S \left[P_1\binom{-\xi(y,l)\sin\theta(y)+}{\eta(y,l)\cos\theta(y)} - P_3\binom{\xi(y,l)\cos\theta(y)+}{\eta(y,l)\sin\theta(y)} \right] N_\theta(y)dldy \qquad (12)$$

Furthermore, the evaluation of the aerodynamic loads is accomplished by the use of single point quadrature over each surface element. Using these aerodynamic loads, the translation and twist of each super element is obtained with respect to the elastic axis of each super element. This is illustrated in Figure 1.

2.3. Moving Grid Techniques

For fluid/structure problems, we must account for grid movement along the deformed surface. Since the structure moves after every time step, we need to accommodate this movement in the CFD domain. This is usually done with some type of dynamics related mesh algorithm For example, Robinson's spring analogy method deals with every grid point like a point mass connected with spring whose stiffness is inversely proportional to the length of the connecting points. More recently, to attack the complex multiblock case, Hartwich and Agrawal (1997), Wong et al. (2000), Reuther and Saunders (unpublished) and Reuther et al. (1996) proposed their own methods. Although they have different forms, they all belong to the transfinite interpolation class. In our computation, we use Hartwich's method to deform the surface points and Reuther's perturbation method to regenerate the volume grid. The moving grid techniques adopted here have been discussed in detail in Lian et al. (2001).

2.4. Interfacing technique:

Developing an interfacing technique to interact back and forth between the fluid-structure model poses the greatest challenge in the field of CAE. The most difficult part of handling numerically the fluid/structure coupling stems from the fact that the structural equations are usually formulated with material (Lagrangian) coordinates, while the fluid equations are expressed using spatial (Eulerian) coordinates. As the two grids are different, one being a finite volume grid and other being a finite element grid, the two types of grid are not likely to coincide at the same points. The CFD grid needs to be finer than the CSD grid as the flow properties are likely to change a lot in vicinities of

4

large gradients. Hence, some kind of interpolation needs to be done between the grids to match the aerodynamic forces from the CFD grid onto the CSD grid. Along the same lines, once the displacement field is obtained from structure solver, data needs to be extrapolated from the CSD grid to the CFD grid. Several methods have been formulated thus far for the interfacing technique. Smith et al. (2000) provides an excellent review of a few interface methods.

Most of the methods mentioned in Smith et al. (2000) gave instabilities at sharp corners while performing interpolation and extrapolation. Since we use a structured volume grid for CFD mesh and QUAD4 for the FEM mesh, we employ a simple bilinear interpolation and linear extrapolation schemes, which was found to be accurate for our case.

Before we proceed to do the necessary interpolation and extrapolation, we need to develop a database that aids us in maintaining a one-to-one correspondence between the CFD and CSD grid points, so that interpolation and extrapolation becomes more straightforward. Since we assume that the wing's cross-section does not change at all time, this simplifies the interpolation schemes to some extent. The fluid/structure interface can be defined as a 2-D surface and hence we can use bilinear interpolation techniques to transfer the loads from CFD mesh onto the CSD mesh. This is done by locating the four points in the CFD grid enclosing a given CSD grid point and interpolating the pressure from the CFD grid points onto the corresponding CSD grid point.

Once the structural calculations are done, we have the displacement and twist of each airfoil section about its elastic axis. We extrapolate these displacements onto the CFD grid based on a method developed by Brown (1997). Since the shape of the airfoil does not change, we know that each of the surrounding points for a given section is going to undergo the same displacement and twist with respect to the elastic axis i.e., each section is going to move like a rigid body. Thus, we extrapolate the displacement fields to points on each section with respect to their respective elastic axis. The value of displacement and twist is obtained at each of the spanwise locations for the CFD mesh by employing linear interpolation and the new geometry for the CFD mesh is obtained therein.

Having performed the data transferring, our focus now shifts towards combining the two modules, viz., CFD and CSD, in time to perform an unsteady CAE calculation. This can cause potential problems as we use different numerical procedures for each module because of higher order stiffness associated with the

matrices in the structures solver. Also, the time scales are very different between the two modules since the CFD module uses an implicit time marching scheme whereas the CSD scheme uses an explicit method. Since the structure solver uses an explicit time marching scheme, it is limited by stability condition with the largest admissible time step. The time step for structure solver is typically orders of magnitude lesser than fluid time step. For the unsteady computations that will be performed, this time step limit does not impose any large increase in CPU usage since the computational effort to solve the iterative scheme of the structure is very small compared to that of the flow solver. Since the fluid and structure formulations need to exchange information to ensure convergence, this procedure needs to be repeated several times before each global time step.

3. Computational Procedure:

The overall computational procedure can be divided into 4 major steps. They are listed below:

Step 1: Perform CFD computation on a 3-D wing to obtain aerodynamic forces on the surface of the wing for a time step

Step 2: Interpolate aerodynamic forces onto the structural mesh

Step 3: Iterate the structure solver a thousand times to obtain the deformation of the wing geometry corresponding to a fluid time step

Step 4: Extrapolate the displacement and twist to obtain the new CFD surface grid

Step 4: Remesh CFD grid based on the deformation obtained from the FEM calculations
These steps are then repeated for subsequent time steps as we march in time. This procedure can be put in the form of a flow diagram as shown in Figure 2.

3.1 Computational Grids:

We now look at the different grid systems employed by both CFD and CSD modules for the AGARD wing geometry. Since the flow solver and structural solver make use of different approaches to solve the governing equations, we need to generate separate meshes for each module. The CFD grid is usually finer when compared to the CSD grid. We generate the mesh system using the AGARD 445.6 wing geometry. The AGARD 445.6 wing is a semispan model with a NACA 65A004 airfoil cross section, which has a 45-degree

American Institute of Aeronautics and Astronautics

quarter-chord sweep angle, an aspect ratio of 1.65 and a taper ratio of 0.66.

3.1.1. CFD Grid:
We develop a CFD mesh around an AGARD 445.6 wing with a non-dimensionalised chord length of 1 unit. The wing is placed in the middle of the y=0 plane of the computational domain, which has dimensions of 10x5x5. The geometry can be designed by either ICEMCFD or PATRAN, the latter being more efficient. Based on the geometry defined, the commercial software ICEMCFD is used to generate high quality grid. The computational domain is divided into 10 blocks. As a first step, we use a coarse mesh, which has 4838 points distributed over the wing surface, or the interface of fluid and structure. The CFD surface grid along with the meshing system at the leading and trailing edges are shown in Figure 3. The entire grid system has a total of 322,622 points.

3.1.2. FEM Grid:
Based on the geometry mentioned above, a surface mesh is created for the wing using shell elements. The finite element mesh is generated using PATRAN and has 2501 points on the surface of the wing. The grid is shown in Figure 4. As can be seen, it contains far less points than that of CFD mesh. In addition, the structural model is divided into 40 super-elements, which are comprised of linear finite elements incorporating Bernoulli-Euler beam bending and torsion acting about the elastic axis of the wing. Each super-element has 20 surface elements, each of which is defined by four nodes.

4. Results and Discussion

We now present the results to demonstrate the fluid-structure interaction in two different scenarios. First, we consider the AGARD 445.6 wing to demonstrate the fluid-structure interaction on a 3-D wing, which undergoes bending and torsion wherein the cross-section moves like a rigid body. Secondly we demonstrate the interaction between the fluid and flexible structure on a flexible membrane wing used in micro air vehicles.

4.1. AGARD 445.6 wing in turbulent fluid flow

In our ongoing effort to develop a complete CAE model, we have made advances thus far to validate our code for performing the necessary interfacing technique. We carry out an unsteady, viscous, turbulent flow calculation on the AGARD wing with a Reynolds number of 366,000, which is in agreement with the experimental setup. We use a time step size of 0.0018 for the flow solver and a step size of 1.8×10^{-6} for the structure solver, which is 1/1000th of the flow time step

used. This choice of structure time step arises from the fact that an explicit central difference scheme is used for the structural solver. In order to ensure stability, the time step, Δt, must be smaller than a critical time step, Δt_{cr}, defined to be T/π (Bathe, 1982) where T is the period of the largest natural frequency of the structure. Using the mass and stiffness matrices generated for the tested model, the highest frequency is found to be 1.6781×10^5 Hz. The critical time step for this model is found to be 1.8969×10^{-6} seconds. We iterate the structure solver a thousand times for every fluid time step in order to make it coincide with the fluid time step.

We ran the code for a number of time steps, updated the mesh after every time step using the deforming mesh algorithm. Figure 5 shows the deflection of the wing in the spanwise direction at four different time instances with increasing time as indicated by the arrowhead. Displacement contours on the surface of the wing at these corresponding time instances are also shown in Figure 6. As can be seen from the figure, the deflection at the wing tip increases with increasing time. A magnified three-dimensional wing shape to clarify the dominance of two bending modes is shown in Figure 7 (a) and (b). Figure 7 (a) depicts the transient response at t=0.012 in which the response is dominated by the second bending mode whereas figure 7 (b) shows the transient response at t=0.043 which illustrates the predominance of first bending mode. The pressure coefficients at different spanwise locations on the top and bottom surface of the wing at different time instants are shown in Figure 8. Also shown in figure is the pressure contour on the surface of the wing at a given time instant. This is in good agreement with Lee-Rausch and Batina (1993) for the given turbulent Reynolds number.

4.2. Membrane Wing in a laminar fluid flow

Beside the fluid and rigid structure interaction, we also investigate the interaction between a flexible structure and its surrounding fluid flow. In our computations we will study the performance of a flexible membrane wing in a steady fluid flow (Ifju et. al., 2002). The membrane wing has a chord length of 5.4 inches and a span of 6 inches. There are three carbon fibers per semi-span of the wing which remain fixed during flight. The overall skeleton of the wing is shown in Figure 9. Typically it flies at angle of attack of 6° with a speed of 10 m/s. The resulting chord Reynolds number is 6×10^4. To investigate the mutual interaction between the flexible structure and the fluid, a dynamic membrane model was proposed by Lian et. al (2000). This model can handle relatively large displacement of the

membrane wing. We use finite element method for the membrane wing shape change and a pressure-based flow solver to calculate the aerodynamic load on the membrane wing. An unstructured mesh, generated for the FEM model, is shown in Figure 10. It has 1030 elements and 1098 nodes on the semi-span of the wing. Streamlines demonstrating the tip vortex are shown in Figure 11. It is interesting to see that the pressure at the leading edge, at this angle of attack, is larger at the top than that at bottom as can be seen in Figure 12. This will eventually cause a kink at the leading edge of the membrane wing. Even in the steady fluid flow, due to the nonlinear dynamic behavior of the membrane, the membrane vibrates with uneven frequencies. We show the displacement of the trailing edge in Figure 13 at different time instances. The vertical dotted lines represent the position of the carbon fibers in the wing.

5. Summary and Conclusions

Two kinds of fluid-structure interaction, one between rigid structure and fluid and other between flexible structure and fluid, were studied in this paper. The rigid structure interaction was demonstrated using the AGARD wing model whereas the flexible structure interaction was studies using the membrane wing model of a micro air vehicle. The algorithm used for the aeroelastic computations incorporated a deforming mesh algorithm and a structure solver in addition to the existing pressure-based flow solver.

Unsteady aeroelastic computations were performed for both laminar and turbulent flows. Two different mode shapes are shown for the AGARD wing model. The pressure coefficient plots for both kinds of flows illustrated the cross over of lines near the leading edge which eventually lead to a kink in the membrane shape but this was not encountered for the AGARD wing as we assumed the cross-section to be rigid. Work is in progress to include compressibility effects in the flow code and to incorporate history dependent structural effects including hysteresis and load stiffening in the structural model.

Acknowledgment

References

Bathe, Klaus-Jurgen (1982) "Finite Element Procedures in Engineering Analysis", Prentice-hall inc., New Jersey.

Bennett, R. M. and Edwards, J. W. (1998) An Overview of Recent Developments in Computational Aeroelasticity, *AIAA-98-2421*.

Brown, S. A. (1997) Displacement Extrapolation for CFD+CSD Aeroelastic Analysis, *AIAA-97-1090*.

Cunningham. H. J., Batina, J. T. and Bennett, R. M. (1988) Modern Wing Flutter Analysis by Computational Fluid Dynamics Methods, *J. Aircraft*, v. 25, n. 10, pp. 962-968.

Farhat, C. and Lesoinne, M. (2000) Two efficient staggered algorithms for the serial and parallel solution of three-dimensional nonlinear transient aeroelastic problems, *Comput. Methods Appl. Mech. Engg.*, n. 182, pp. 499-515.

Hartwich, P. M., and Agrawal, S. (1997) Method for Perturbing Multiblock Patched Grids in Aeroelastic and Design Optimization Applications, *AIAA Paper 97-2038*.

Ifju, P., Jenkins, D., Ettinger, S., Lian, Y., and Shyy, W. (2002), Flexible-Wing-Based Micro Air Vehicles, 40th AIAA Aerospace Sciences Meeting & Exhibit, AIAA. Paper 2002-0705.

Lee-Rausch, E. M. and Batina, J. T. (1993) Calculations of AGARD Wing 445.6 Flutter using Navier-Stokes Aerodynamics, *AIAA-93-3476*.

Lian, Y., Steen, J., Trygg-Wilander, M., and Shyy, W. (2001) Low Reynolds Number Turbulent Flows around a Dynamically Shaped Airfoil, *AIAA-2001-2723*.

Lian, Y., Shyy, W., Ifju, P., and Verron, E., Fluid-Structure Interaction of a Membrane Wing for Micro Air Vehicle Applications, AIAA Paper, 2002.

Liu, F., Cai, J., Zhu, Y., Wong, A. S. F. and Tsai, H. M., (2000) Calculation of Wing Flutter by a Coupled CFD-CSD Method, *AIAA-2000-0907*.

Reuther, J., and Saunders, D., Analytic Mesh Perturbation Algorithm for Aerodynamic Shape Optimization (Unpublished).

Reuther, J., Jameson, A., Farmer, J., Martinelli, L., and Saunders, D. (1996) Aerodynamics Shape Optimization of Complex Aircraft Configurations via an Adjoint Formulation, *AIAA Paper 96-0094*.

Robinson, B. A., Batina, J. T. and Yang, H. T. Y. (1991) Aeroelastic Analysis of Wings Using the Euler Equations with a Deforming Mesh, *J. Aircraft*, v. 28, n.

11, pp. 781-788.

Shyy, W. (1994) "Computational Modeling for Fluid Flow and Interfacial Transport", Elsevier, Amsterdam.

Shyy, W., Thakur, S.S., Ouyang, H., Liu, J. and Blosch, E. (1997) "Computational techniques for Complex Transport Phenomena", Cambridge University Press, New York.

Smith, M. J., Hodges, D. H. and Cesnik, C. E. S., (2000) Evaluation of computational Algorithms Suitable for Fluid-Structure Interactions, *J. Aircraft*, v. 37, n. 2, pp. 282-294.

Soulaimani, A., (2000) A Finite Element Based Methodology For Computational Nonlinear Aeroelasticity, *AIAA-2000-2335*.

Thakur, S. and Wright, J. (1999) "STREAM: A Computational Fluid Dynamics and Heat Transfer Code for Complex Geometries. Part 1: Theory. Part 2: User's Guide" Streamline Numerics, Inc., Gainesville, Florida.

Wong, A.S.F., Tsai, H.M., Cai, J., Zhu, Y. and Liu, F. (2000) Unsteady Flow Calculations with a Multi-Block Moving Mesh Algorithm, *AIAA-2000-1002*.

Yates, E. C., Jr., (1987) AGARD *Standard Aeroelastic Configuration for Dynamic Response, Candidate Configuration I.-Wing 445.6*, NASA TM 100492.

Table 1: Table of a few existing aeroealstic models

Author's Name (year)	Description of work	Main Results
Cunningham, Batina, Bennett (1988)	- Computational scheme for transonic aeroelastic analysis - Transonic small disturbance formulation - Equations of motion are based on the natural vibrational modes of the aircraft - Time marching flutter analysis – Linear potential equation that models wing as a flat plate – Non-linear equation incl. Wing thickness - AGARD configuration with 45 deg sweep angle and M=0.338-1.141	- Aerodynamic forces and flutter characteristics obtained using linear formulation compared well with expt. - Non-linear flutter results compared well with expt but not so with linear results - Can treat configurations with arbitrary lifting surfaces
Schuster, Vadyak, Atta (1990)	- A 3-D flow solver coupled with linear static structural model to study aeroelastic response of aircraft - Grid deflection method is used to update the grid after each time step. - CFD solver: ENS3D - Swept, tapered wing with constant cross-section with M=0.9 and α=9 deg was used - Wing mesh: 92 x 32 x 32 points	- Aeroelastic analysis compared well with experiment with respect to pressure coefficient and twist - Flexible wing/body configuration gave better results compared to rigid body configuration - Separation on the upper surface was not predicted
Guruswamy Byun (1993) Guruswamy Byun (1994)	- Compute aeroelasticity by direct coupling using time-integration method - Fluid: Euler equations/N-S equations - Structure: Plate finite elements - Aerodynamic loads are transferred by bilinear interpolation and by virtual surface methods - CFD grid (151 x 30 x 35) - FEM grid (36 plate elements) - Fighter type wing with M=0.854 and α=1 deg.	- Validity of coupling plate elements with Euler equation - Virtual surface method transfers loads more accurately than bilinear interpolation technique

8

Table 1 (contd.): Table of a few existing aeroealstic models

Author's Name (year)	Description of work	Main Results
Bhardwaj, Kapania, Reichenbach, Guruswamy (1998)	• Static aeroelastic solutions using a linear structural model. • Flow solver: NASTD • FEM solver: NASTRAN • F-18 wing with M=0.95 and α=1 deg. • CFD and CSD gird points are matched directly • CFD grid (800,000 points) • FEM grid (2000 nodes)	• Maximum deflection compares well with prev. analytical results • Convergence of struc. code is very fast • Inc. accuracy of direct finite element displacement data compared to modal analysis • Aeroelastic coupling is not as efficient as a completely integrated scheme
Lewis and Smith (1998)	• External aeroelastic simulation for internal aerodynamics and shell structures • Coupled set of structure and flow equations • Predictor-corrector scheme for structural integration • Solver used: ENS3DAE • Tested on an engine liner to study flutter with M=0.7 in inner region and M=0.4 in the annular region	• Results showed the engine liner to be dynamically stable • Inner flow mach no. had little effect on aeroelastic response • Effect of pressure loadings on the shell structures were not considered in this method
Patil, Hodges, Cesnik (1999)	• Non-linear aeroelastic model for complete aircraft model for high AR wings • Mixed variational formulation of beams in moving frames • Finite-state airloads for deforming airfoils on fixed wings • Linear and non-linear analysis were considered for comparative study • Rigid and flexible wings were compared • High-altitude, low-endurance aircraft is considered for performing tests	• Linear analysis produced almost identical results for frequencies of the beam for flutter calculations • Flutter speed and freq was found to be less than that predicted by linear model • Flight dynamics changed considerably for flexible wings • The steady state solution and the frequency modes were affected by wing flexibility
Patil, Hodges (2000)	• Theoretical non-linear aeroelastic analysis of high AR wings to investigate effects of geometrical nonlinearity • Structural solver: nonlinear mixed variational formulation • Aero solver: 3-D nonplanar double lattice theory • Rigid slender wing with semi-span AR=16 and flexible wing with α=10 • Grid: steady: 16 x 1; unsteady: 48 x 6	• Structural nonlinearity, nonplanar geometry and 3-D effects have little effect on a rigid wing • Nonplanar geometry and struc nonlinearity have negligible effect on flexible wings too • A decrease in flutter speed with increase in wing loading was noted for flexible wings
Garcia, Guruswamy (1999)	• Model for coupled nonlinear beam FEM model with N-S solver for static aeroelastic analysis of high AR wings • Flow solver: ARC3D fluids module of ENSAERO-WING code • Structural code: NASTRAN • Aeroelastic research wing (ARW-2) @ M=0.85 and α=2	• FEM results are accurate except for deflections which were smaller than modal results • Nonlinear and linear beam models predicted similar pressure coeff results • Geometrical nonlinearity was found to be negligible

9

American Institute of Aeronautics and Astronautics

Table 1 (contd.): Table of a few existing aeroealstic models

Author's Name (year)	Description of work	Main Results
Soulaimani (2000)	• Methodology for non-linear computational aeroelasticity • Flow solver: FEM based 3-D Euler and N-S eqns. For unstructured meshes with ALE formulation for moving grids • Structure: Commercial FEM code • Coupling: Partitioned solution procedures for time integration • M=0.96 and α=0 on a AGARD-445.6 • Unstructured Grid (84946 points)	• The FEM based scheme developed is found to be qualitatively similar to the finite volume schemes
Farhat and Lesoinne (2000)	• Serial and Parallel methodologies for nonlinear transient aeroelastic problems • Arbitrary Lagrangian-Euler equations are incorporated into the unstructured flow solver • Deforming mesh algorithm was used to enable grid movement • M=0.901 on an AGARD wing	• Partitioned algorithms were found to be efficient than monolithic schemes

Table 2: Description of existing CAE methods for an AGARD wing

Author	CFD solver	Deforming mesh algorithm	Structural solver	Interfacing technique
Cunningham et al (1988)	TSD	None	Modal Analysis	none
Robinson et al. (1991)	Euler	Spring analogy	Modal analysis	none
Lee-Rausch and Batina (1993)	Navier-Stokes	Spring analogy	Modal analysis	none
Soulaimani (2000)	FEM based	ALE formulation	Commercial code	none
Liu, et al. (2000)	Euler	TFI method	Modal equations of motion from FEA	Spline methods
Farhat and Lessoine (2000)	Unstructured Navier-Stokes	ALE formulation	Finite element based solver	Conservative method
Our approach	**Full Navier-Stokes**	**TFI method**	**Bernoulli-Euler beam equations**	**Linear interpolation extrapolation**
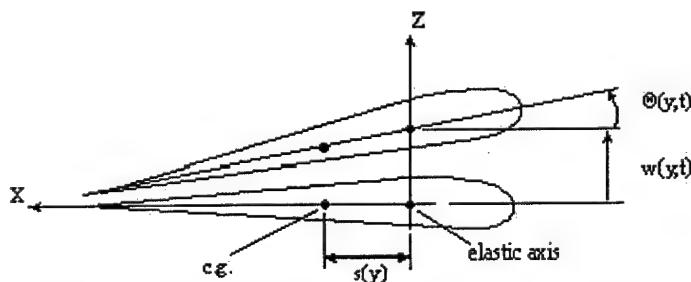
Figure 1. Displacements Measured with respect to the Elastic Axis

American Institute of Aeronautics and Astronautics
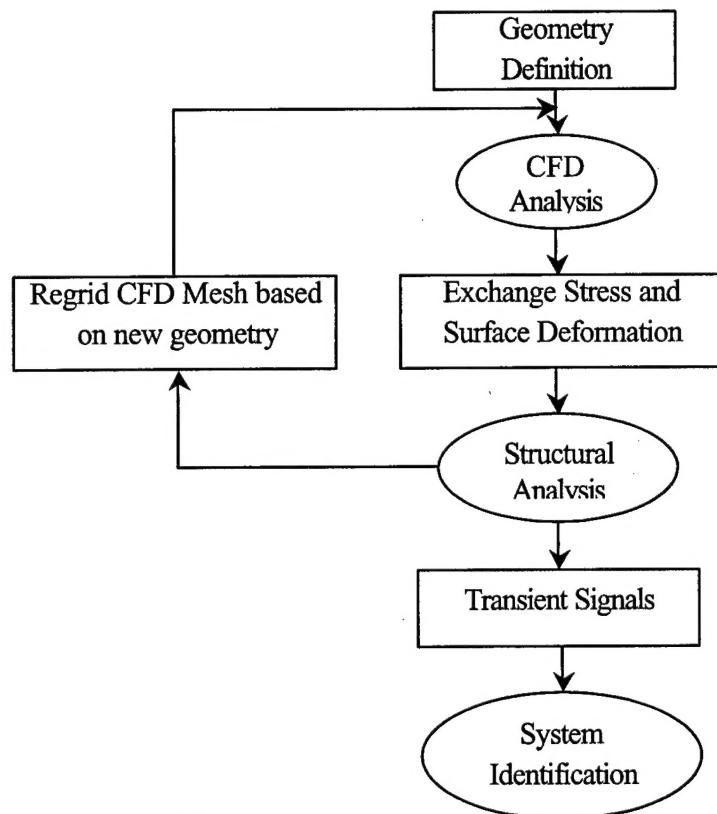
Figure 2. Computational Aeroelasticity analysis block diagram for time-domain analysis
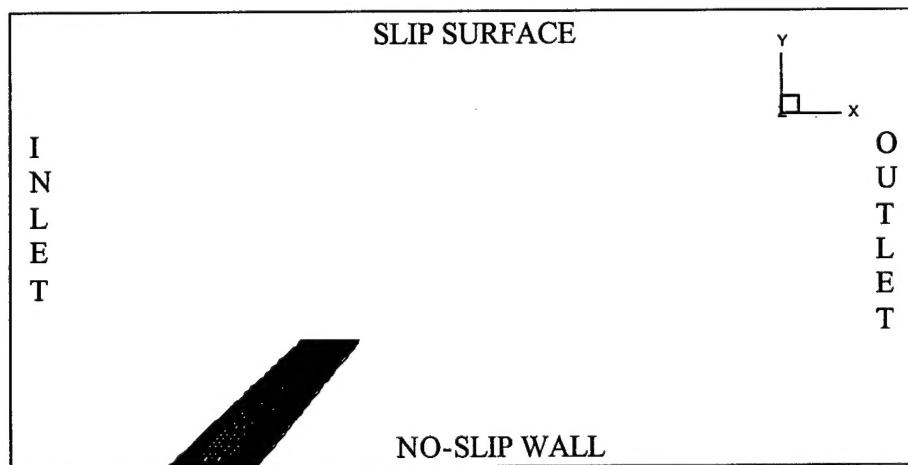
Figure 3. Top view of AGARD wing along with flow domain and corresponding boundary/initial conditions

American Institute of Aeronautics and Astronautics
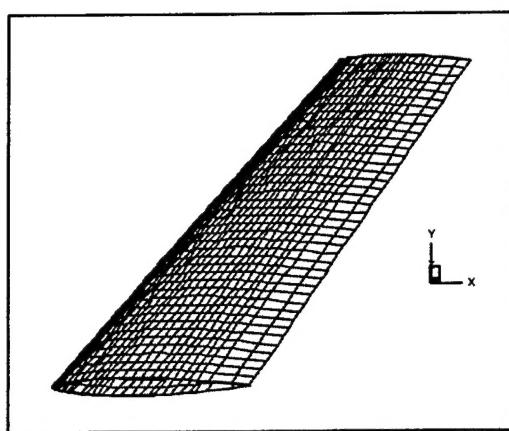
**Figure 4.** FEM structural grid on the AGARD wing
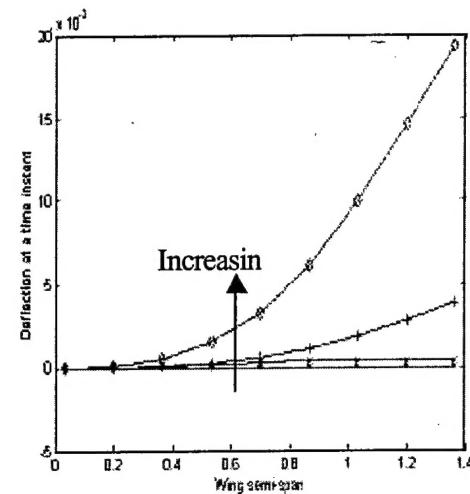
Figure 5. Deflection of the wing in the spanwise direction at four different time instants
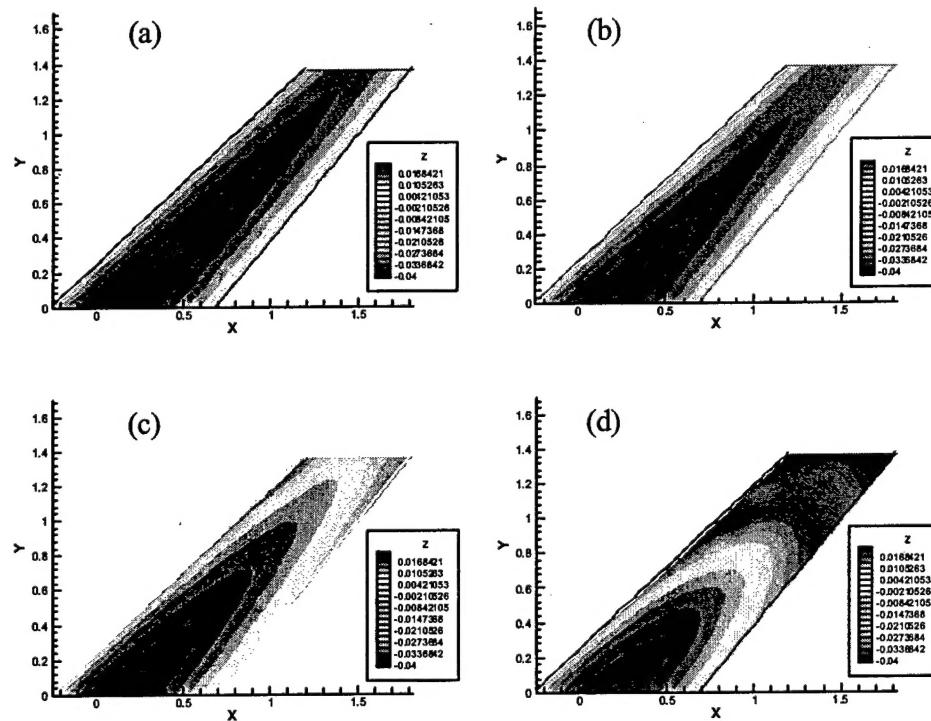

Figure 6. Displacement contours on the AGARD wing at the corresponding time instants shown in Figure 1. (a) through (d) represents increasing time.

12

American Institute of Aeronautics and Astronautics

(a)

(b)
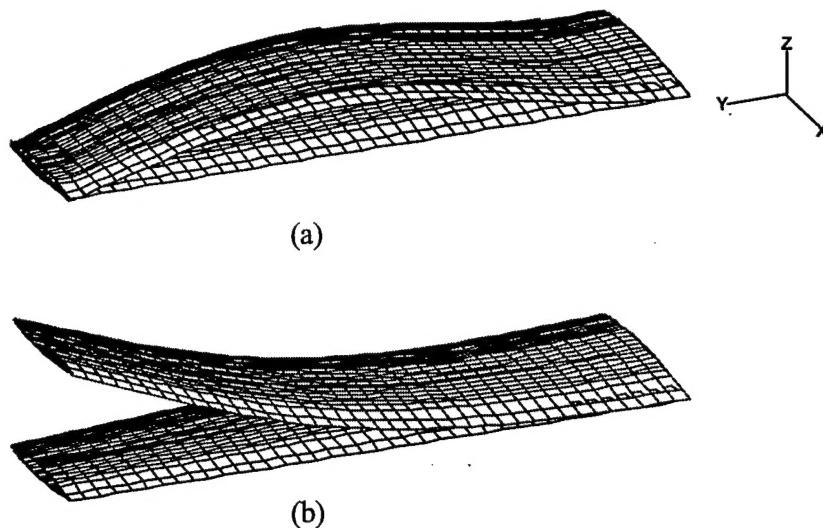
Figure 7. Magnified 3-D shape of the wing at two different time instants demonstrating the transient response (a) at t=0.012 s depicting dominance of second bending and (b) at t=0.043 s depicting dominance of first bending.
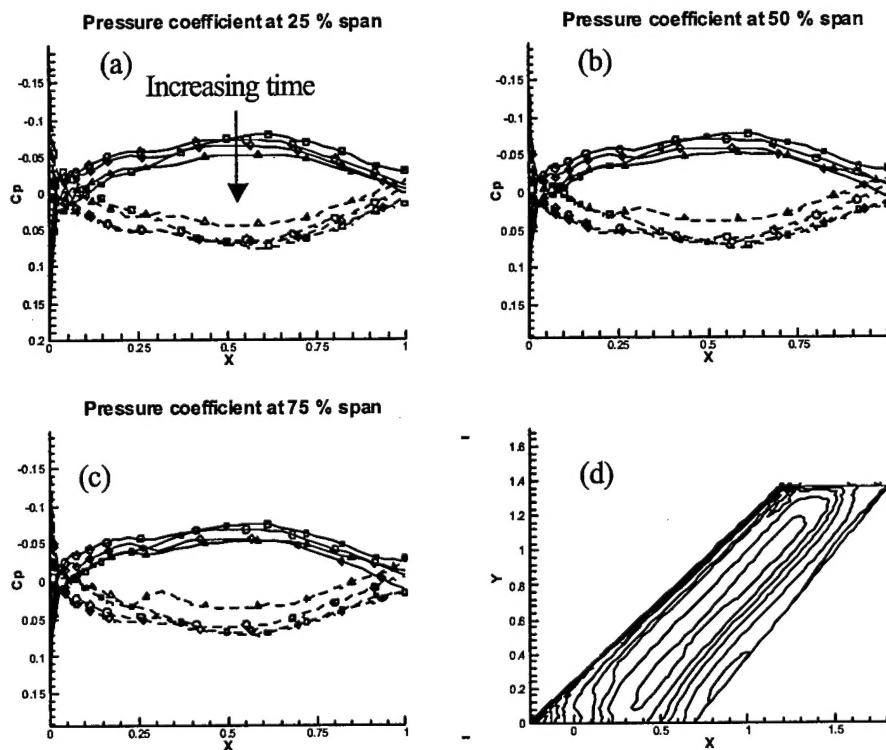
Figure 8. (a), (b), (c) Pressure contours at 25%, 50% and 75% span for 4 different time instants respectively. (d) Pressure contour on the surface of the wing.

13

American Institute of Aeronautics and Astronautics
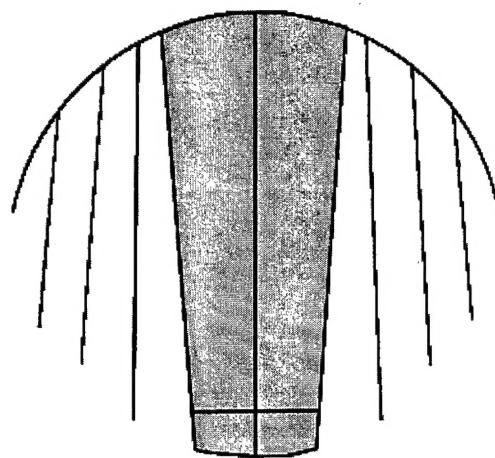
Figure 9. Skeletopn of the membrane wing showing the carbon fibers

Figure 12. Pressure distribution along the streamwise direction at t=0.22.

Figure 10. Unstructured finite element grid for the membrane wing
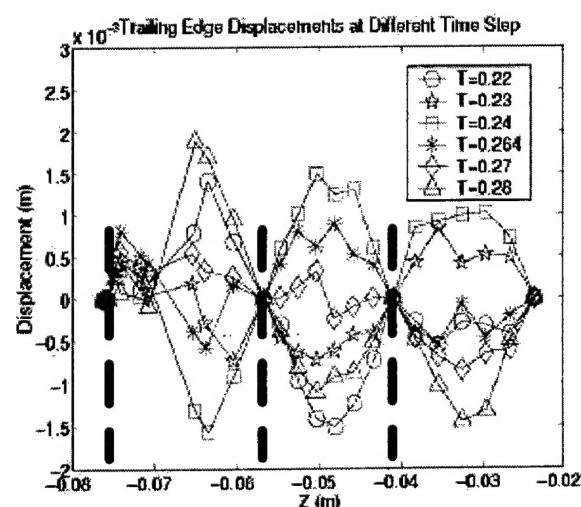

Figure 13 Trailing edge displacement of the membrane wing at different time step.

Figure 11. Streamlines around the rigid wing at angle of attack 6°.

14